POINT CLOUD GROUND SEGMENTATION ALGORITHM OF VINEYARD AGRICULTURAL ROBOT BASED ON SURFACE FITTING
/
基于曲面拟合的葡萄园农业机器人点云地面分割算法

Fa SUN, Fanjun MENG, Mengmeng NI, Zhisheng ZHAO, Lili YI
Shandong University of Technology, Collage of Agricultural Engineering and Food Science, Zibo, China
Corresponding author: Lili YI; Tel: +86 18553308656; E-mail: yili0001@sdut.edu.cn
DOI: https://doi.org/10.35633/inmateh-76-06

Keywords: *Vineyard robot, Surface fitting, Ground division, Moving least squares*

ABSTRACT

To address the autonomous navigation and operation requirements of agricultural robots in complex terrain environments of vineyards, this report proposes a point cloud Ground segmentation algorithm based on surface fitting, aiming to solve the problems of reduced segmentation accuracy and insufficient adaptability of traditional planar assumption methods in unstructured terrains such as sloped fields and ridge furrows. The core of the algorithm lies in adopting a point cloud representation method based on a non-uniform polar grid, which dynamically allocates face element sizes according to point cloud density and the width between vineyard ridges, effectively addressing the issues of point cloud sparsity and representability. Subsequently, the moving least square method is used to fit surface models. During the fitting process, strategies such as Gaussian weight function, cosine and sine basis functions, and set of orthogonal functions are introduced to shorten the algorithm's running time and reduce computational complexity. The algorithm's performance is evaluated on the public dataset KITTI and in real-world environments, and compared with algorithms such as RANSAC, GPF, R-GPF, and Patchwork. Experimental results show that the proposed algorithm outperforms other algorithms in both Precision and Recall. In practical environments, the algorithm can accurately and effectively segment complex vineyard environments, meeting the operational requirements of agricultural robots and providing technical support for the advancement of smart agriculture.

摘要

针对葡萄园复杂地形环境下农业机器人自主导航与作业的需求，本文提出了一种基于曲面拟合的点云地面分割算法，旨在解决传统平面假设方法在坡地、垄沟等非结构化地形中存在的分割精度下降与适应性不足的问题。算法的核心在于采用一种基于非均匀极坐标网格的点云表示方法，该方法根据点云密度以及葡萄园垄间宽度动态分配面元大小，有效解决了点云稀疏性和可表示性问题；随后用移动最小二乘法拟合曲面模型，在拟合过程引入高斯型权函数、正余弦基函数，正交函数集的策略，缩短算法运行时间，降低计算复杂度。在公开数据集 KITTI、葡萄园环境中评估算法性能，并于 RANSAC、GPF、R-GPF、Patchwork 等算法进行对比。实验结果表明，本文算法在 Precision 和 Recall 均优于其他算法；葡萄园环境中，该算法能准确、有效的分割葡萄园复杂环境，满足农业机器人的作业需求，为推进智慧农业提供了技术支撑。

INTRODUCTION

Agriculture, as the foundational industry underpinning socio-economic development, holds paramount significance in China—a nation with a millennia-old agrarian civilization. The development of agriculture not only determines national food security and social stability, but also serves as a pivotal driver for economic growth and rural revitalization.

In recent years, autonomous driving technology has been developing rapidly, and its research and application have become a core topic in the field of intelligent transportation systems *(Avcı et al., 2024)*. Driven by multiple factors such as algorithm optimization, hardware upgrading, and data-driven, self-driving vehicles have made significant progress in the key technical aspects of perception *(Cong et al., 2024)*, decision-making *(Wang et al., 2024)* and control *(Vidano et al., 2024)*. As the first step of an autonomous driving system, the accuracy of environment sensing is directly related to the performance and safety of the whole system. Among many sensors, LiDAR has become a key component for autonomous driving environment sensing with its advantages of high accuracy *(Wu et al., 2024)* and long-range measurement *(Bayer et al., 2021)*. Light Detection and Ranging (LiDAR for short) is an active remote sensing technology that utilizes laser pulses to measure distances in order to obtain three-dimensional positional information about the target object and

generate high-precision three-dimensional point cloud data. On this basis, the ground segmentation algorithm employs multi-dimensional feature analysis and deep learning framework to achieve accurate recognition of ground and non-ground points in complex terrain.

In a vineyard environment, the ground can have slopes or weeds, etc., that are more rugged than urban transportation surfaces. Weeds, fallen leaves, and highly reflective objects (metal supports, plastic film) can cause noise in LIDAR scans, and fragmented vegetation makes the ground segmentation unclear, as well as surrounding objects, blocking the fit, conventional ground segmentation algorithms selectively exclude it, and this algorithm is optimized for these characteristics. The main contributions are as follows:

1) Dynamic area optimization, improving the traditional fixed-area selection mode and adjusting the scanning focus according to the vineyard environment: the nearest area and the farthest area, it improves the plant recognition accuracy by 7.3%, reduces the leakage rate to 2%, and can detect obstacles as early as possible to provide safe time for the subsequent path planning.

2) Dual noise reduction technology, incorporating multipath reflection suppression and sensor dynamic compensation, the noise false detection rate is reduced by 78.8% and the terrain detection error is optimized by 61.7% under dense foliage and high temperature environments.

3) Design of fast surface fitting algorithms based on orthogonal basis functions: by replacing the traditional planar model with Legendre orthogonal polynomials and combining circular radial weight functions with matrix-free inverse least squares solving, the computational complexity is reduced from $O(n^3)$ to $O(n^2)$, which ensures the accuracy of complex terrain fitting while shortening the computation time of a single frame to 35ms to meet the real-time demand of 10 Hz for agricultural robots.

MATERIALS AND METHODS

Most of the traditional algorithms are adapted to urban traffic surfaces, and the orchard environment is relatively more complex. The ground segmentation algorithm proposed in this paper is based on concentric zone model (CZM), and several key modules are set up to realize the extraction of ground information from radar point cloud. CZM utilizes a uniform polar grid representation to divide the point cloud into multiple fan-ring regions with regularity and orientation, and the density of each region can be set by adjusting the parameters. Key modules include Reflected Noise Removal (S-RNR), Vertical Interference Removal (S-VIE), Sub-Regional Partitioning (SRP), Surface Model Fitting (S-SSF), Adaptive Thresholding (ATS), and Temporal Ground Recovery (TGR).

The overall framework is shown in Figure 1, and the following paragraphs highlight the definitions and rationale for the core modules.

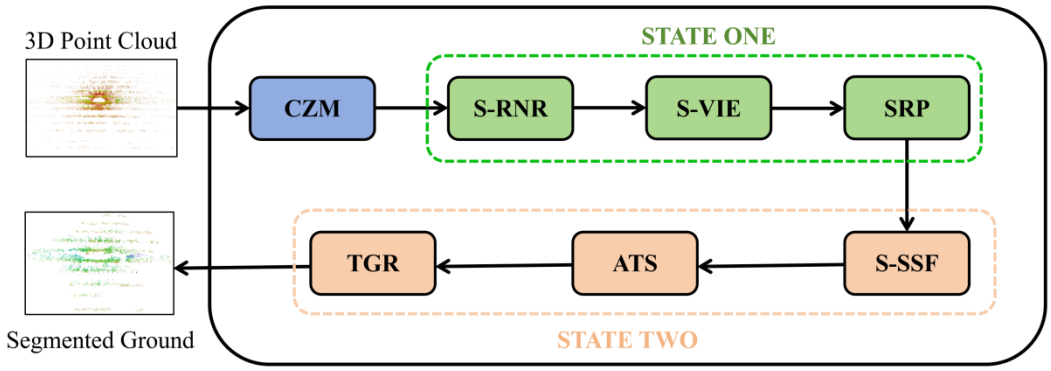

Fig. 1 - Module Flowchart

Concentric Zone Model (CZM)

When dealing with point cloud data of complex terrain, especially vineyard pavements, most of the traditional algorithms designed for flat urban pavements rely on fixed strategies such as adaptive binning and quadratic distributions and assume locally flat ground to simplify the computation. However, the ground is usually not flat and the density of the point cloud data varies with distance, which leads to under- or over-segmentation problems when conventional methods are ineffective in dealing with sparse and under-represented point clouds.

In response to these problems, a uniform polar grid model is proposed, which divides the point cloud collection into multiple sector-ring regions by radial distance and azimuth. However, there are two main problems with this method: the fan ring area near the center is small and has a sparse number of points, while the area away from the center is similarly underpopulated due to a sparse point cloud, both of which affect the accuracy of the ground plane fitting.

To overcome these limitations, the CZM was used. The model parametrically adjusts the density of the sector ring region in each ring band, taking into account the problem of LIDAR being dense in the near and sparse in the far, ensuring that the ring bands have a reasonable number of sector rings regardless of the distance from the center. The model is defined as follows:

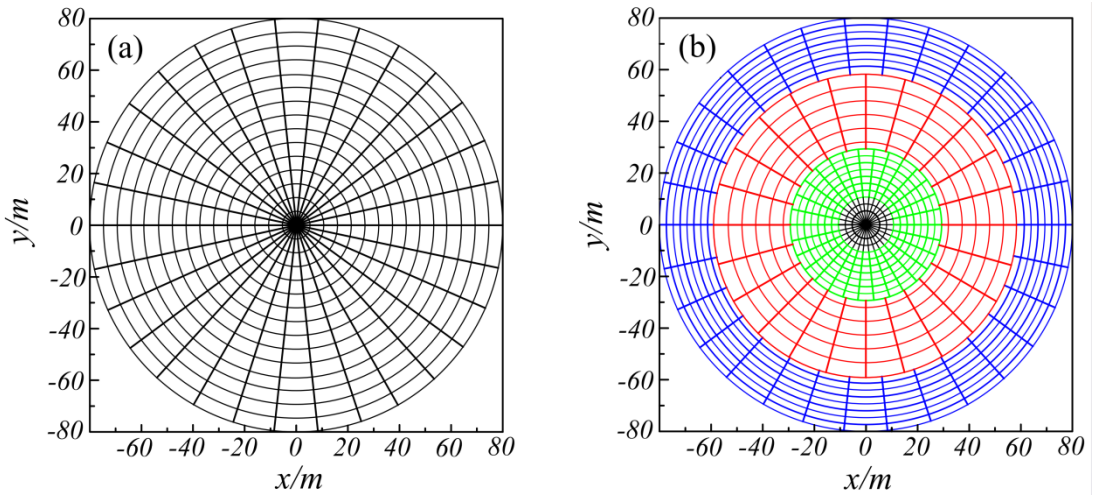

Fig. 2 - (a)Tradition modeling method; (b)concentric zone model

Compared with the traditional model definition Fig. 2(a), Fig. 2(b) is more applicable to the orchard environment by detailing the distant sparse point cloud and the point cloud in the vicinity of the LiDAR, the former confirms that obstacles can be detected in advance for subsequent path planning, while the latter detects obstacles at close range.

Reflected Noise Removal (S-RNR)

The presence of highly reflective objects (metal brackets, plastic films), radius effects (e.g., multiple reflections from plant leaves), and sensor noise in the vineyard point cloud collection can generate noise, these noise points can significantly affect the reliability of the fitted ground plane. Noise points also occur below the ground plane, as shown in Figure 3.

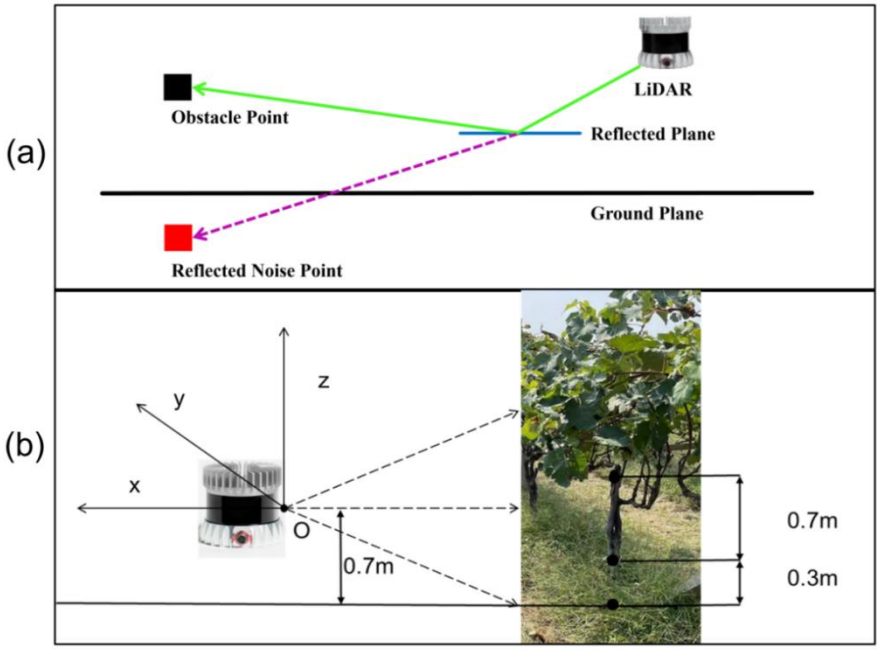

Fig. 3 - (a)Point Cloud Reflection Noise Schematic Diagram; (b)LiDAR Position Schematic Diagram

As shown in the figure, the height of the LIDAR mounted on the wheeled robot is 0.7 m. Let the height threshold be h, with the point O as the origin and the positive direction of the z-axis. Let the height of the point x in the vineyard LiDAR point cloud be z_x, then the equation of the non-ground point will be:

$$z_x > h \tag{1}$$

According to the actual measurement, the weed height of standardized planting vineyard is about 0.3 m, then the threshold is -0.4, then the vineyard LiDAR point cloud can be left when the height is greater than -0.4, otherwise it is separated as a ground point.

In order to solve the noise point problem, the algorithm employs the Regional Reflected Noise Removal (R-RNR) module and introduces the introduction of multipath effect suppression and sensor noise compensation. R-RNR performs reflection noise removal for each sector-ring region separately, searching for all points in the point cloud below a specified height one by one, and identifying points with reflection intensity below a threshold as reflection noise points. Multipath effect suppression establishes a three-frame sliding window that rejects transient points (e.g., vignette points from blade jitter) that persist for <0.3 seconds:

$$\mathrm{P_{valid}} = \{\mathrm{p_i} \mid \sum_{\mathrm{t=1}}^{3} \mathrm{I}\,(\mathrm{p_i} \in \mathrm{F_t}) \geq 2\} \tag{2}$$

Where $\mathrm{F_t}$ denotes the t-th frame point cloud, the suspected multipath point is detected by reverse ray detection, and if there is an occluder (e.g., a leaf point cloud) on the path from the sensor to the point, it is determined as a fictitious point and rejected. Sensor noise compensation, on the other hand, is applied by applying a nonlinear compensation model through a temperature sensor that collects the ambient temperature T in real time:

$$\mathrm{I_{corrected}} = \mathrm{I_{raw}} - \mathrm{k_1 e^{k_2 T}} \tag{3}$$

where $\mathrm{k_1}$=0.03 and $\mathrm{k_2}$=0.12 are the calibration parameters. And the point cloud motion compensation model was constructed by combining the IMU data, and the extended Kalman filter (EKF) was used to estimate the real spatial coordinates of each point:

$$\hat{\mathrm{x}}_\mathrm{t} = \mathrm{x_{meas}} - \int_{\mathrm{t-\Delta t}}^{\mathrm{t}} \mathrm{v}(\tau)\mathrm{d}\tau \tag{4}$$

where $\mathrm{v}(\tau)$ is the instantaneous speed of the agricultural vehicle.

Surface model fitting (S-SSF)

Moving least squares provides an effective polynomial approximation strategy for high-precision surface fitting of scattered point clouds, centered on minimizing the sum of squared node errors. When applied to LiDAR point cloud data, it generates smooth and close fitting surfaces. However, facing the huge amount of point cloud data, the traditional methods have high computational complexity. For this reason, the fast moving least squares method is used to simplify the coefficient matrix solution using weighted orthogonal functions (considering only diagonal elements and avoiding inverse), which significantly improves the computational efficiency and meets the real-time demand of automatic driving while ensuring the accuracy.

The fitting function is expressed as:

$$\boldsymbol{f}(\mathbf{x},\mathbf{y}) = \sum_{\mathbf{i=1}}^{\mathbf{m}} \boldsymbol{\alpha_i}\,(\mathbf{x},\mathbf{y})\mathbf{p_i}(\mathbf{x},\mathbf{y}) = \mathbf{p^T}(\mathbf{x},\mathbf{y})\boldsymbol{\alpha}(\mathbf{x},\mathbf{y}) \tag{5}$$

It can be simplified as follows:

$$f(\mathrm{t}) = \sum_{\mathrm{i=1}}^{\mathrm{m}} \alpha_\mathrm{i}\,(\mathrm{t})\mathrm{p_i}(\mathrm{t}) = \mathrm{p^T}(\mathrm{t})\alpha(\mathrm{t}) \tag{6}$$

where $\mathrm{t}=(\mathrm{x},\mathrm{y})$ and the coordinates t as a function of:

$$\alpha(t) = [\alpha_1(\mathrm{t}), \alpha_2(\mathrm{t}), \ldots\ldots, \alpha_\mathrm{m}(\mathrm{t})]^T \tag{7}$$

The basis function is a complete polynomial of order k and m is the number of terms in the product function:

$$\mathrm{p}(\mathrm{t}) = [\mathrm{p_1}(\mathrm{t}), \mathrm{p_2}(\mathrm{t}), \ldots\ldots, \mathrm{p_m}(\mathrm{t})]^\mathrm{T} \tag{8}$$

For surface fitting, a two-dimensional basis function is required, and the basis function $\mathrm{p}(\mathrm{t})$ takes the form:

Linear base: $\mathrm{p}(\mathrm{t}) = [1, \mathrm{x}, \mathrm{y}]^\mathrm{T}$

Secondary base: $p(t) = [1, x, y, x^2, xy, y^2]^T$

In the moving least squares approximation, the coefficient is determined by minimizing the weighted sum of squares of the errors of the nodes of the approximation function in a neighborhood of point x:

$$J = \sum_{I=1}^{n} w(x)[f(t) - Z_I]^2 = \sum_{I=1}^{n} w(x)[\sum_{i=1}^{m} p(t_I)\alpha(t_I) - Z_I]^2 \quad (9)$$

where n is the number of nodes affected in the neighborhood of x, Z_I is the value of the node at $t = t_I$, and $x = t - t_I$ is the difference between the two points, $t\text{-}t_I = \sqrt{(x - x_I)^2 + (y - y_I)^2}$, $w(x) = w(t\text{-}t_I)$ is the weight function of node t_I.

When the above equation equals zero, J reaches a minimum value and hence the following can be obtained:

$$\sum_{I=1}^{n} w(x)[\sum_{i=1}^{m} p(t_I)\alpha(t_I) - Z_I]^2 = 0 \quad (10)$$

$$\sum_{I=1}^{n} w(x) \sum_{i=1}^{m} p(t_I)\alpha(t_I) = \sum_{I=1}^{n} w(x) * Z_I \quad (11)$$

$h(x)$ and $g(x)$ are introduced to simplify the expression:

$$(h, g) = \sum_{i=1}^{n} w(x - x_i)h(x_i)g(x_i) \quad (12)$$

$$\alpha_1(t)(p_i, p_1) + \alpha_2(t)(p_i, p_2) + \cdots .. + \alpha_n(t)(p_i, p_n) = (p_i, Z), i = 1,2 \ldots, m \quad (13)$$

Organized into a system of linear equations, also known as normal equations:

$$\begin{bmatrix} (p_1, p_1) & (p_1, p_2) & \cdots & (p_1, p_m) \\ (p_2, p_1) & (p_2, p_2) & \cdots & (p_2, p_m) \\ \cdots & \cdots & \cdots & \cdots \\ (p_m, p_1) & (p_m, p_2) & \cdots & (p_m, p_m) \end{bmatrix} \begin{bmatrix} \alpha_1(t) \\ \alpha_2(t) \\ \cdots \\ \alpha_m(t) \end{bmatrix} = \begin{bmatrix} (p_1, Z) \\ (p_2, Z) \\ \cdots \\ (p_m, Z) \end{bmatrix} \quad (14)$$

Solving the above system of linear equations yields the reformation coefficient a(t) at node t. If the basis function $p_i(t)(i = 1,2,3, \ldots, m)$ is taken to be the set of orthogonal functions of the point set $\{x\}$ and the weight $\{w_i(i = 1,2,3, \ldots, m)\}$, we obtain:

$$(p_k, p_j) = \sum_{i=1}^{n} w_i\, p_k(t_i)\, (t_i) = \begin{cases} 0 & , (k = j) \\ A_k & , (k \neq j) \end{cases} (k, j = 1,2 \ldots m) \quad (15)$$

Then the matrix can be obtained:

$$\begin{bmatrix} (p_1, p_1) & 0 & \cdots & 0 \\ 0 & (p_2, p_2) & \cdots & 0 \\ \cdots & \cdots & \cdots & \cdots \\ 0 & 0 & \cdots & (p_m, p_m) \end{bmatrix} \begin{bmatrix} \alpha_1(t) \\ \alpha_2(t) \\ \cdots \\ \alpha_m(t) \end{bmatrix} = \begin{bmatrix} (p_1, Z) \\ (p_2, Z) \\ \cdots \\ (p_m, Z) \end{bmatrix} \quad (16)$$

Then one can solve for $\alpha_i(t)(i = 1,2,3 \ldots, m)$:

$$\alpha_i(t) = \frac{(p_i, Z)}{(p_i, p_i)} \quad (17)$$

Collation is available:

$$f(t) = \sum_{i=1}^{m} p_i(t) \cdot \frac{\sum_{I=1}^{n} w(t - t_I)\, p_i(t_I)}{(p_i, p_i)} = \sum_{I=1}^{n} O_I^k(t) Z \quad (18)$$

where the form function is:

$$O_I^k(t) = w(t - t_i) \sum_{i=1}^{m} \frac{p_i(t) p(t_I)}{(p_i, p_i)} \quad (19)$$

By integrating the set of orthogonal functions, matrix inversion can be avoided, thereby resolving the problem of matrix irreversibility, reducing the computational time of the least squares method, and lowering overall algorithmic complexity.

In the moving least squares method, the choice of the weight function is crucial, and in a complex orchard environment, the appropriate weight function greatly affects the smoothness of the fitted ground. The weight function $w(t\text{-}t_i)$ in the moving least squares method should be tightly supported, that is, the weight

function is not equal to zero in a subdomain of x, and is zero outside of this subdomain, which is called the support domain of the weight function (i.e., the region of influence of x).

Therefore, a circular support domain with radius r was selected for the weight function, where $d = t\text{-}t_i$, $\bar{r} = \frac{d}{r}$.

This choice ensures that the function values at each node are influenced only by data points within the circular support domain, while points outside this region have no impact. Due to the compact support of the weight function, only the data points within the region of influence affect the value at point x. The weight function $w(t\text{-}t_i)$ is required to be non-negative and monotonically decreasing as d^2 increases. In this study, a two-part Gaussian-type weight function is used in place of the traditional three-part moving least squares (MLS) weight function. This modification results in a smoother fit, reduces fitting time, and lowers algorithmic complexity.

The Gaussian-type weight function is shown in equation (20):

$$\bar{w}(\bar{r}) = \begin{cases} \frac{e^{-\beta^2\bar{r}^2} - e^{-\beta^2}}{1 - e^{-\beta^2}} & , \bar{r} \leq 1 \\ 0 & , \bar{r} > 1 \end{cases} \quad (20)$$

RESULTS

Data set

In this paper, tests are performed using datasets collected by two different devices.

1) KITTI point cloud public dataset, the data acquisition equipment for the U.S. Velodyne company HDL-64 type 3D mechanical rotation Lidar, with 64 lasers, acquisition frequency of 10 Hz, each frame produces about 130,000 scanning points, the effect of the dataset is shown in Figure.

2) The vineyard dataset was collected using the OSI-64 LiDAR, which has a measurement range of 120 meters, a vertical viewing angle of 45°, a horizontal viewing angle of 360°, a rotation angle of 360°, a vertical angular resolution of 0.52°, a horizontal resolution of 1024, and 131072 sampling points per second, with data effects as shown in Fig.4.

(a) (b) (c)

Fig. 4 - (a)Sample Images of the KITTI Dataset; (b)OSI-64 3D LiDAR; (c)Vineyard Dataset Rendering

Algorithm testing

1) Hardware platform

In this study, the KOMODO-03 general-purpose tracked robot mobile chassis developed by Extreme Robotics Technology Co. The chassis is fully electrically powered with a 48V 50Ah Li-ion battery power system with a maximum operating voltage of 54.6 V and a discharge cut-off voltage set at 43 V. The power section consists of two DC brushless motors and two 15:1 gearboxes. The computer is equipped with an AMD R7-4800H processor, 16 GB RAM and a single NVIDIA GeForce GTX1650ti GPU.

The mobile chassis structure is shown in Figure 5.

Fig. 5 - Tracked mobile platform for orchard operation robots

1. External Monitor; 2. Jetson AGX Xavier; 3. Crawler-Type Mobile Chassis; 4. Dual-Antenna GNSS-RTK; 5. 64-Line 3D LiDAR.

2) Measurement indicators

For the evaluation of segmentation accuracy, it is mainly evaluated from Precision, Recall and F1 Score, and the calculation method of each evaluation index is shown below:

$$\mathrm{Precision} = \frac{N_{TP}}{N_{TP} + N_{FP}} \tag{21}$$

$$\mathrm{Recall} = \frac{N_{TP}}{N_{TP} + N_{FN}} \tag{22}$$

$$F1 = 2 * \frac{\mathrm{Precision} * \mathrm{Recall}}{\mathrm{Precision} + \mathrm{Recall}} \tag{23}$$

where: N_{TP} is the number of ground points correctly labelled; N_{FN} is the number of ground points incorrectly labelled as non-ground points; N_{FP} is the number of non-ground points incorrectly labelled as ground points; and N_{TN} is the number of non-ground points correctly labelled.

KITTI dataset testing

The Semantic KITTI dataset is a large-scale dataset designed for autonomous driving scenarios, and in order to validate the accuracy of the algorithms in this paper for ground point cloud segmentation, this dataset was used to evaluate the performance of the proposed algorithms versus existing algorithms for ground segmentation.

In this experiment, the first 100 frames were selected (i.e., numbered 01 to 100) from the KITTI dataset as the test object, and each frame contains about 130,000 cloud data points. In order to make a clear comparison of the point cloud data, the non-ground point cloud was labelled as red and the ground point cloud as green, and the effect of the delineation of the road information was visualized by rviz.

The effect diagram of road information division is shown in Fig. 6, and the algorithm of this paper is compared with four ground segmentation algorithms of RANSAC *(Martin et al., 1981)*, GPF *(Dimitris et al., 2017)*, R-GPF *(Hyungtae et al., 2021)* and Patchwork *(Hyungtae et al., 2021)*. The comparison test is shown in Fig. 7, and the segmentation accuracy is shown in Table 1.

Table 1

Ground segmentation accuracy

Algorithm	Precision	Recall	F1 Score
RANSAC	0.8452	0.8389	0.8417
GPF	0.9256	0.7962	0.8551
R-GPF	0.7678	0.8862	0.8228
Patchwork	0.9279	0.9245	0.9267
Ours	0.9469	0.9458	0.9479

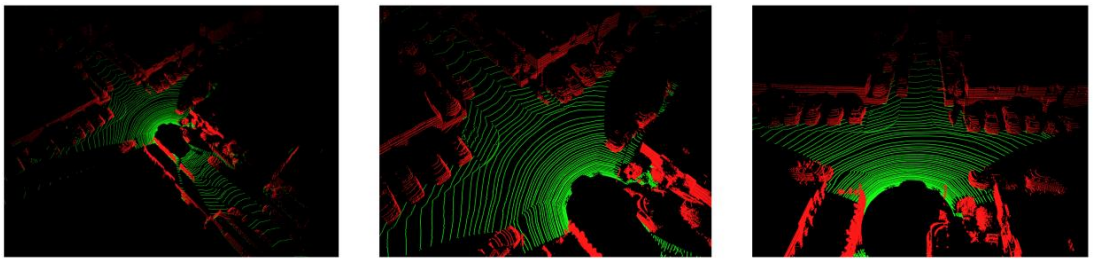

(a) (b) (c)

Fig. 6 - (a)Urban environment scene; (b), (c) Local vehicle scene

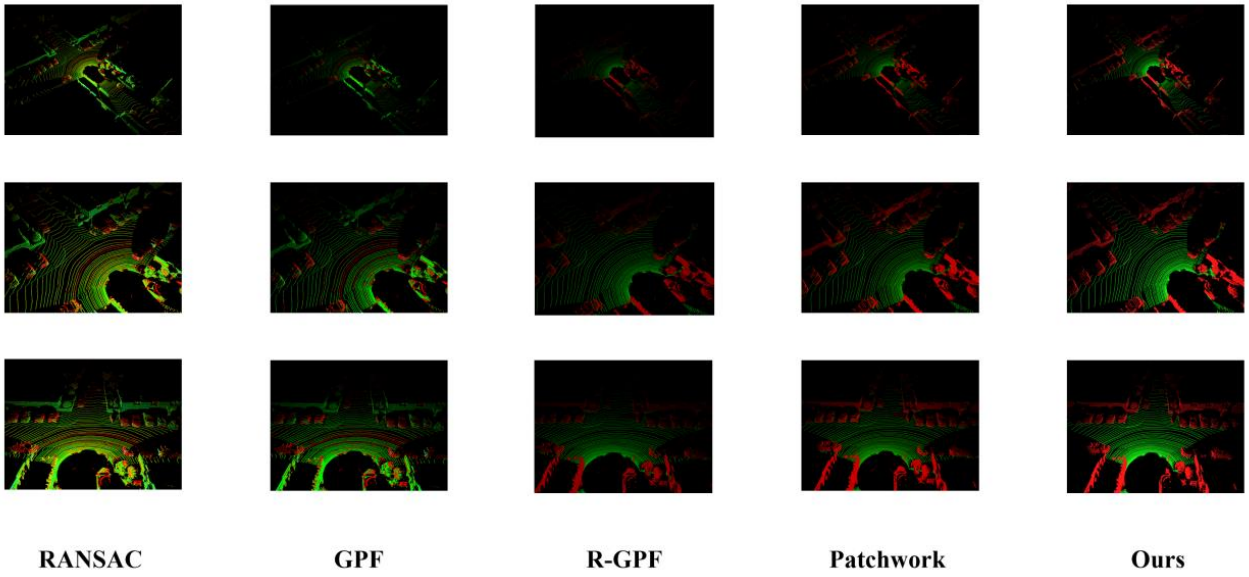

Fig. 7 - KITTI data set comparison test

In Fig. 7, the green point cloud represents the ground point cloud and the red point cloud represents the non-ground point cloud, and it can be seen by the global segmentation information as well as the local segmentation details that the algorithm in this paper is better than the other four algorithms. The ground segmentation accuracy in Table 1 shows that the algorithm in this paper is better than the above four algorithms in terms of segmentation accuracy, precision, recall, and accuracy in road tests in urban environments.

Vineyard Data Testing

The initial design of the algorithm in this paper is applied to the vineyard, using the OSI-64 LiDAR in the actual vineyard scene to collect data, and the original data and the algorithm of this paper to segment the environment comparison, the comparison effect graph is shown in Figure 8.

Figure 8 shows the real environment algorithm test, the test scene is a vineyard road, and 8(a)(d) shows the actual scene, where there is a human-type obstacle in (a), which is used to test the segmentation effect of the algorithm. Figure 8(b)(e) shows the unsegmented point cloud scene of the vineyard. Figure 8(c)(f) shows the scene after segmentation by the algorithm, and it can be seen from the segmentation effect that the algorithm in this paper can segment accurately.

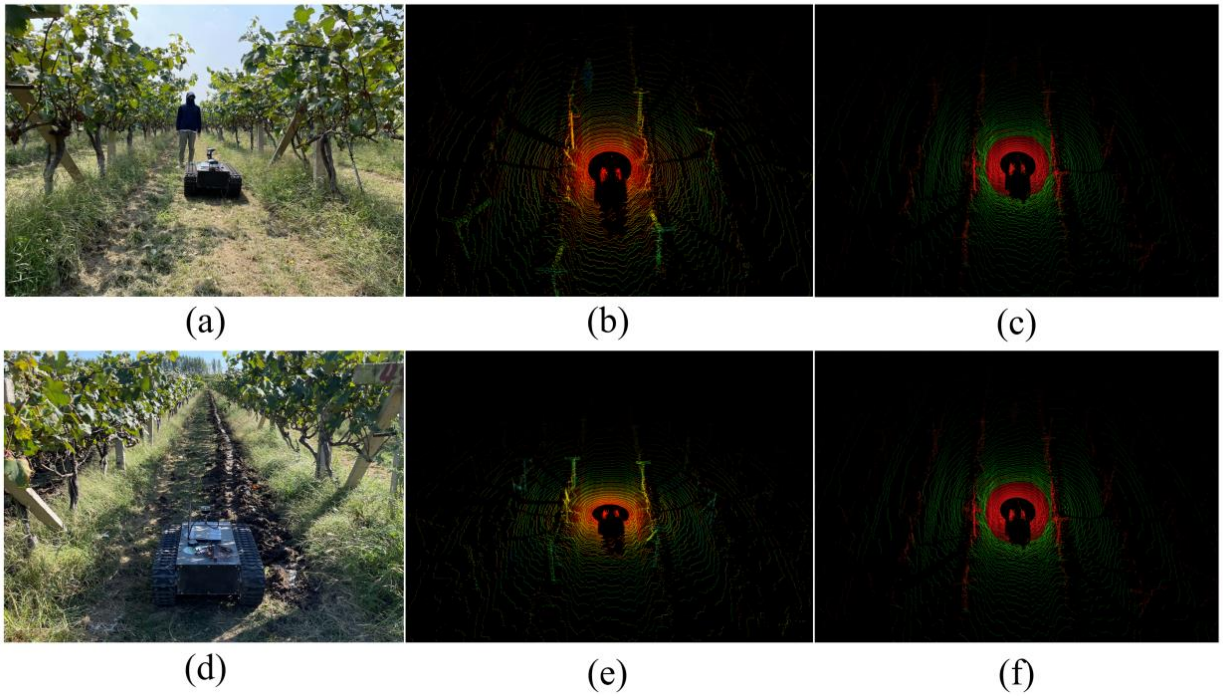

Fig. 8 - Real environment algorithm testing

CONCLUSIONS

Aiming at the problem of insufficient performance of traditional methods for point cloud segmentation in complex scenes in vineyards, this paper proposes a surface-fitting ground segmentation method. By using orthogonal function basis to improve the moving least squares method, the computational complexity is reduced so as to improve the speed of surface fitting, Gaussian-type weight function is introduced to solve the problem of non-smoothness of the fitted surface, and the sine-cosine basis function is introduced, which is more able to restore the original shape of the vineyard ground. By improving the search area range of the radar so that the point cloud focuses on the farthest and nearest regions, obstacles can be detected as early as possible, providing sufficient time for path planning. Dual noise reduction technology is used to integrate multipath reflection suppression and sensor dynamic compensation to reduce the false detection rate of noise and enhance the robustness of ground segmentation in vineyard scenes.

The superiority of this approach is validated through experiments on the KITTI dataset and real vehicles. The results show that the method achieves accurate segmentation of ground point cloud, which is better than RANSAC, GPF, R-GPF and Patchwork algorithms. The segmentation precision can reach 0.9469 and the recall can reach 0.9458.

In future work, multimodal data fusion of LiDAR with visual and inertial measurement unit (IMU) data will be explored to enhance the robustness of the algorithm in complex environments such as rain, fog, and nighttime conditions. Additionally, the algorithm will be extended to other agricultural scenarios, including terraces and orchards, to evaluate its generalization performance.

ACKNOWLEDGEMENT

The project supported by the R&D of low-speed unmanned autonomous navigation controller Project under Grant (No.2022TSGC1175).

REFERENCES

[1] Alherimi N, Saihi A, Ben-Daya M. (2024) A Systematic Review of Optimization Approaches Employed in Digital Warehousing Transformation. *IEEE Access* 12, 145809-145831.

[2] Avcı İ, Koca M. Intelligent Transportation System Technologies, Challenges and Security. In: *Applied Sciences*; 2024.

[3] Bayer MM, Li X, Guentchev GN, Torun R, Velazco JE, Boyraz O. Single-shot ranging and velocimetry with a CW lidar far beyond the coherence length of the CW laser. *Opt Express* 2021; 29(26):42343-42354.

[4] Cong P, Feng H, Li S, Li T, Xu Y, Zhang X. A visual detection algorithm for autonomous driving road environment perception. *Engineering Applications of Artificial Intelligence* 2024; 133:108034.

[5] Deng W, Chen X, Jiang JJE. A Staged Real-Time Ground Segmentation Algorithm of 3D LiDAR Point Cloud. 2024.

[6] Dimitris Z, Izzat I, Nikolaos P. Fast segmentation of 3D point clouds: A paradigm on LiDAR data for autonomous vehicle applications, 2017 *IEEE International Conference on Robotics and Automation* (ICRA), 2017.

[7] Firkat E, An F, Peng B, Zhang J, Mijit T, Ahat A, et al. FGSeg: Field-ground segmentation for agricultural robot based on LiDAR. *Computers and Electronics in Agriculture* 2023; 211:107965.

[8] Huang J, Zheng Z, Zhang Y, Zhou Y. Segmentation Clustering Algorithm for Point Cloud Processing of Targets on The Ground. *Journal of Physics: Conference Series* 2023; 2478.

[9] Hyungtae L, Sungwon H, Hyun M. ERASOR: Egocentric ratio of pseudo occupancy-based dynamic object removal for static 3D point cloud map building. *IEEE Robotics and Automation Letters*, 2021.

[10] Hyungtae L, Minho O, Hyun M. Patchwork: Concentric zone-based region-wise ground segmentation with ground likelihood estimation using a 3D LiDAR sensor. *IEEE Robotics and Automation Letters*, 2021.

[11] Itakura K, Miyatani S, Hosoi F. Estimating Tree Structural Parameters via Automatic Tree Segmentation From LiDAR Point Cloud Data. *IEEE J. Sel. Top. Appl. Earth Obs. Remote Sens*., 2022; 15:555-564.

[12] Jiang X, Xie Y, Na C, Yu W, Meng Y. Algorithm for Point Cloud Dust Filtering of LiDAR for Autonomous Vehicles in Mining Area. *Sustainability* 2024, 16, 2827.

[13] Jin R, Ren M. Background extraction and ground segmentation method based on Roadside LiDAR. *Computer and Digital Engineering* 2023; 51(9):2033-2037+2054.

[14] Martin A, Robert C. Random Sample Consensus: A Paradigm for Model Fitting with Applications to Image Analysis and Automated Cartography. *Communications of the ACM*, 1981.

[15] Petrakis G, Partsinevelos P. Lunar ground segmentation using a modified U-net neural network. *Machine Vision and Applications* 2024; 35(3):50.

[16] Vidano T, Assadian F. Control Performance Requirements for Automated Driving Systems. In: *Electronics*; 2024.

[17] Wang C, Morris JT, Smith EM. A Lidar Biomass Index of Tidal Marshes from Drone Lidar Point Cloud. *Remote Sens.* 2024, 16, 1823. https://doi.org/10.3390/rs16111823

[18] Wang Y, Han Z, Xing Y, Xu S, Wang J. A Survey on Datasets for the Decision Making of Autonomous Vehicles. *IEEE Intelligent Transportation Systems Magazine* 2024; 16(2):23-40.

[19] Wang X, Ma X, Li Z. Research on SLAM and Path Planning Method of Inspection Robot in Complex Scenarios. *Electronics* 2023, 12, 2178. https://doi.org/10.3390/electronics12102178.

[20] Wu L, Chen Y, Le Y, Qian Y, Zhang D, Wang L. A high-precision fusion bathymetry of multi-channel waveform curvature for bathymetric LiDAR systems. *International Journal of Applied Earth Observation and Geoinformation* 2024; 128:103770.

[21] Zhu M, Zhang B, Zhou C, Zou H, Wang X. Target Recognition of Multi Source Machine Vision Pan Tilt Integrated Inspection Robot for Power Inspection. *IEEE Access* 2024; 12:45693-45708.